ACS OMEGA

http://pubs.acs.org/journal/acsodf

Article

Green Assembly of Covalently Linked BiOBr/Graphene Composites for Efficient Visible Light Degradation of Dyes

Weiwei Tie, Surjya Sarathi Bhattacharyya, Cancan Han, Shuaibiao Qiu, Weiwei He,* and Seung Hee Lee*

Cite This: *ACS Omega* 2022, 7, 35805−35813

Read Online

ACCESS | Metrics & More | Article Recommendations

ABSTRACT: A novel high-performance BiOBr@graphene (BiOBr@G) photocatalyst with a new assembly structure had been demonstrated using a facile hydrothermal method through chemical bonding of reduced graphene oxide and structure-defined BiOBr flakes for improving charge separation and transfer performance, which were first synthesized at room temperature in immiscible solvents without corrosive acids. The prepared samples were characterized, and the BiOBr@G composite realized an efficient assembly portfolio of graphene and BiOBr flakes with defined structures, verified by scanning electron microscopy (SEM), transmission electron microscopy (TEM), X-ray diffraction (XRD), and Raman and X-ray photoelectron spectroscopy (XPS), in which BiOBr flakes were covalently linked with the assembled graphene sheets through the Bi−C bond. This composite exhibited remarkable visible light absorbance and efficient photoinduced charge splitting characteristics in comparison with those of pure BiOBr, as established by DRS absorption, photoluminescence radiation, and photocurrent study. Hence, a very small amount (5 mg) of the BiOBr@G composite displayed a complete photodegradation effect on the rhodamine B dye under only 15 min of visible light excitation, which was three times faster than that of pure BiOBr and extremely superior to that of commercial P25. This was probably ascribed to the well-defined BiOBr structure itself, elevated light absorbance, and Bi−C chemical bond inducing quick charge separation and transfer in the BiOBr@G composite. Additionally, investigations on the photocatalytic mechanism displayed that the photogenerated holes in the BiOBr valence band and derivative superoxide radicals played vital roles in the photodegradation of RhB dyes, as reinforced by the electron spin resonance method, where the covalent linking of BiOBr and graphene served as an effective pathway for charge transportation.

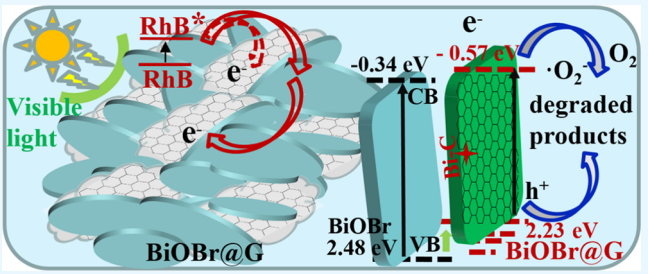

1. INTRODUCTION

Organic dyes and pigments discharged into the environment mixed with industrial wastewater pose threats to human health and Mother Nature.[1,2] Efficient utilization of solar energy in terms of newly developed photocatalytic degradation technology has been identified as a clean and economic approach for toxicity removal from industrial liquid waste and hence reversing or stopping environmental damage.[3−6] Among the various semiconductor photocatalysts that have been developed, including TiO_2, ZnO, Ag_3PO_4, Bi_2WO_6, $BiVO_4$, and others, specific importance has been given to two-dimensional (2D) layered BiOBr fabricated by interleaving $[Bi_2O_2]$ slabs with slabs of double bromine. The band gap and internal interleaving electric field of 2D layered BiOBr are such that considerable photocatalytic activity can be achieved by visible light excitation.[7,8] However, individual BiOBr shows limited photocatalytic activity owing to least efficient captivation of visible light, sluggish charge transfer capability, and nonideal electron−hole pair separation efficiency.[9,10] Hence, research efforts have been made to fabricate composites of BiOBr with functional materials of recent interest such as graphene or graphitic-like flakes for developing advanced photocatalytic decontaminants, which open possibilities to combine favorable characteristics of both the materials.[11−15]

An atomic layer form of carbon with a π-conjugated aromatic structure and sp^2 bonding forms graphene. Additionally, oxygen-containing functional groups distinguish graphene oxide (GO) from graphene. Reduction of GO produces reduced graphene oxide (RGO), and it is commonly used as a precursor for simple and efficient fabrication of optimized composites due to graphene's unique properties such as exceptional electrical conductivity, huge specific surface area, and extraordinary transparency.[16−19] Thus, various BiOBr−

Received: June 24, 2022
Accepted: September 13, 2022
Published: September 26, 2022

https://doi.org/10.1021/acsomega.2c03965
ACS Omega 2022, 7, 35805−35813

graphene composites have been fabricated to enhance the photocatalytic activity of BiOBr.[12−15,17] According to previous reports, most BiOBr−graphene composites focus on the formation of inorganic BiOBr nanocrystals by selectively loading onto the graphene surface via a free nucleation and growth process in a mixed solution of metal salts and graphene oxide (GO).[13,15,17] However, this technique has few possible downsides. First of all, only a portion of the graphene sheet surface can be covered by discrete BiOBr nanocrystals, and thus, most of the graphene surface remains uncovered and contact interaction between them is also limited, which appears to reduce the composite's photocatalytic activity and active locations.[20] Additional difficulty is imposed by the limited precision to control the morphology and structure of BiOBr nanocrystals due to the uncontrollable compatibilities of the nucleation and growth process of BiOBr crystals and their interaction with GO.[21] Due to these disadvantages, optimum usage of graphene has never been possible, as sheets with limited exposed surface areas and tendency of reaggregation among composite units create difficulties; also, limitations in controlling the loading sites, structure, and morphology of BiOBr nanocrystals on graphene sheets restrict the photocatalytic performances of functional composites. Therefore, fabrication of a new composite structure in which individual graphene sheets can freely suspend or sufficiently interact with BiOBr nanocrystals having a definite degree of crystal face exposure and morphological structure, henceforth eliminating the tendency of restacking BiOBr or graphene sheets, is necessary to improve the photocatalytic performance. To the best of our knowledge, a facile method realizing covalent coupling of BiOBr with a definite morphology structure via chemical bonding fabricated in immiscible solvents without corrosive acids for subsequent self-assembly with graphene has not been previously reported.

Herein, we have described a facile and reproducible two-step route to obtain a new 2D-2D BiOBr@graphene composite (BiOBr@G), in which BiOBr flakes are first synthesized at room temperature in immiscible solvents without corrosive acids or other expensive chemicals. Subsequently, a new 2D/2D composite of BiOBr flakes with well-defined structures modified and surrounded by the assembled graphene sheets via chemical bonding is constructed using a hydrothermal reaction. The composite BiOBr@G may be considered an acceptable nonflexible composite structure, in which BiOBr flakes intensely interact with the assembled graphene sheets through their active sites. Importantly, BiOBr@G exhibits significantly improved photodegradation of the RhB dye compared to that of pure BiOBr and commercial P25. The improved enactment of BiOBr@graphene is mainly attributed to the intrinsic BiOBr flakes and their stiff and efficient connections with graphene sheets, which are advantageous for light absorbance and mobility of charges. The high-performance BiOBr@G photocatalyst fabricated by this simple method is expected to open new opportunities in reversing or stopping environmental damage.

2. EXPERIMENTAL SECTION

2.1. Materials. All chemicals including $Bi(NO_3)_2.5H_2O$, citric acid (CA), *n*-octane, cetyltrimethylammonium bromide (CTAB), silver nitrate, benzoquinone, methanol and t-Butanol, used in this study, were analytical grade and were directly used without further purification as received from Shanghai Aladdin Biochemical Polytron Technology Co. All experiments were performed under ambient temperature and humidity conditions. The graphene oxide dispersion (5 mg/mL) used for preparing BiOBr@G was purchased from XF Nano Technology Ltd. (Nan Jing, China), in which graphene oxide sheets had lateral sizes of 0.5−5 μm and 1−6 layers. Unless otherwise specified, rhodamine B (RhB) and other reagents and materials were obtained commercially from Sinopharm Chemical Reagent Plant (China).

2.2. Preparation of BiOBr Flakes. BiOBr flakes were synthesized by a modified process in an immiscible solvent system.[9] In a typical synthesis process, 0.4851 g of $Bi(NO_3)\cdot 5H_2O$ was dissolved in 7.5 mL of deionized water containing 0.072 g of citric acid, and then, this above-mentioned solution was added drop by drop to 7.5 mL of *n*-octane containing 0.3645 g of CTAB. After 30 min of vigorous stirring at room temperature, the product was finally obtained from its suspension after centrifuging, washing with a mixture of deionized water and ethanol, and further vacuum-drying at 60 °C.

2.3. Synthesis of the BiOBr@graphene Oxide Composite. The BiOBr@ graphene composite was fabricated through a hydrothermal process based on Zhang's work with modification, achieving the effective integration of BiOBr together with reduction of GO for RGO.[18] Briefly, 0.5, 1, or 2 mL of graphene oxide dispersion (5mg/mL) was dispersed in a 30 mL aqueous ethanol solution of H_2O (v/v = 2:1) by a 1 h ultrasonic process; after that, 0.2 g of BiOBr synthesized above was added to the aforesaid aqueous ethanol mixture containing GO and stirred for 1 h to obtain a homogeneous suspension. The suspensions were maintained at 120 °C for 3 h in a 50 mL Teflon-sealed autoclave. Finally, the prepared composites, named as BiOBr@G-0.5mL, BiOBr@G-1mL, and BiOBr@G-2mL, were received after a series of procedures, filtration, washing with deionized water and ethanol, and vacuum drying at 60 °C.

2.4. Characterization. An X-ray diffractometer (D8/Advance) with Cu Kα radiation (λ = 1.5406 Å) was used to obtain X-ray diffraction (XRD) patterns. Laser excitation (532 nm wavelength) in a confocal Raman microscope instrument (Renishaw in Via) was used to record the Raman spectra of the samples. An X-ray photoelectron spectrometer (Thermo Scientific Escalab 250Xi) was used to characterize the sample composition. A field emission scanning electron microscope (Nova Nano SEM 50) and transmission electron microscope (FEI Talos F200X) were used for microscopic morphological characterization. An UV−vis spectrometer (Shimadzu UV-3600plus) was used to record the UV−vis diffuse reflectance spectra (UV−vis DRS). Room temperature photoluminescence (PL) spectra were recorded using a Hitachi F-7000 fluorescence spectrophotometer. Electron spin resonance (Bruker A300-10/12) was used for radical characterization. We have used a traditional three-electrode system using a potentiostat (CH Instruments, CHI 660) (with applied potential 0.2 V, Ag/AgCl reference electrode, platinum counter electrode, and the working electrode prepared with the synthesized samples.) immersed in saturated KCl solution beneath optical irradiation to perform the photocurrent measurement.[22]

2.5. Photocatalytic Activity. Degradation of RhB under visible light irradiation has been used to examine the photocatalytic activities of the sample. The light source in the form of a 300 W xenon lamp with a 420 nm cutoff filter was positioned at a distance of 100 mm from the sample. The

https://doi.org/10.1021/acsomega.2c03965
ACS Omega 2022, 7, 35805−35813

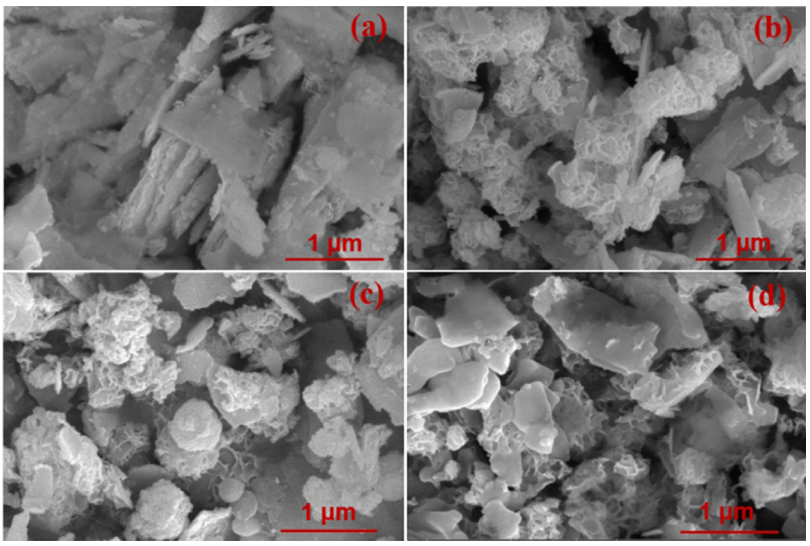

Figure 1. Scanning electron microscopy images of pure BiOBr (a) and BiOBr@G-0.5mL (b), BiOBr@G-1mL (c), and BiOBr@G-2mL (d) composites.

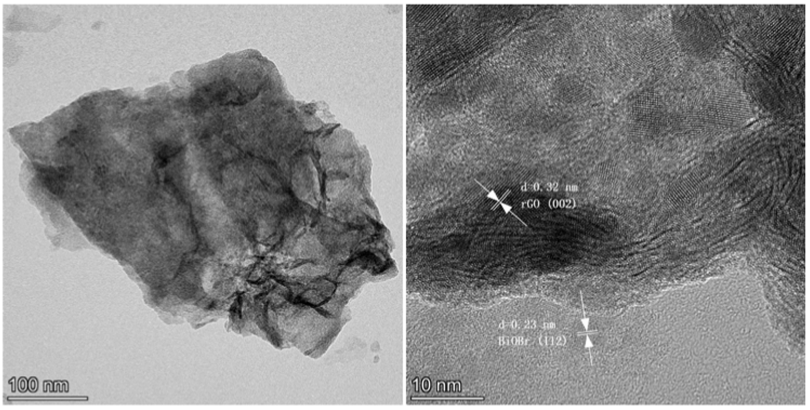

Figure 2. Transmission electron microscopy images of the BiOBr@G composite.

photocatalyst amounting to about 5 mg was added to 50 mL of RhB solution (20 mg L^{-1}). To ensure the establishment of an adsorption/desorption equilibrium, initially, the suspensions were stirred in the dark and then under visible light irradiation. The suspensions were removed from the reactor after a fixed time interval of visible light irradiation and centrifuged to get rid of the remaining photocatalyst powders. The irradiation time-dependent variation of the concentration of RhB remaining in solution was assessed by UV−vis spectroscopy at a typical wavelength of around 553 nm.

3. RESULTS AND DISCUSSION

The morphological microstructural features of pure BiOBr and the BiOBr@G composite are examined with SEM and TEM. Figure 1 shows the SEM images of pure BiOBr prepared in an immiscible solvent system, which consists of large numbers of irregular flat flakes with a lateral size of ∼0.5−1.0 μm stacked over one another (Figure 1a). Strikingly different from the morphology of pure BiOBr, BiOBr@G-0.5mL, BiOBr@G-1mL, and BiOBr@G-2mL composites (Figure 1b,c,d) display similar flakes but a stacked wrinkle texture above or among them. The flakes with a wrinkle-like microstructure of the BiOBr@G composite are further investigated by the TEM measurement. From Figure 2, graphene assemblies on BiOBr flakes or between them and the edge of BiOBr@G-1mL look folded, which is the characteristic feature for graphene sheets.[17] Then, clear lattice fringes for individual BiOBr and graphene are all observed in a high-resolution TEM image. The interfringe spacing for each is about 0.23 and 0.32 nm, which corresponds to the BiOBr (112) plane and graphene (002) plane, respectively, suggesting that this composite has successfully assembled BiOBr and graphene with a close contact.[12,23]

The phase structure and purity of the synthesized samples are investigated by X-ray diffraction (XRD). As shown in Figure 3a, both samples exhibit similar XRD patterns with prominent diffraction peaks at approximately 10.5, 25.3, 32.3, 39.5, 46.5, 57.3, and 66.7°, corresponding to the planes of (001), (011), (110), (112), (020), (212), and (220), respectively. The diffraction peaks can be indexed to the tetragonal phase of BiOBr (JCPDS No.73−2061), and no other diffraction peaks are observed, assuring the phase purity of the sample.[24] However, no distinct diffraction peak is noticed for nanocrystalline graphite (d_{002} around 25°), ascribed as the over-stacked graphene layers in the composite, which may be attributed to the low loading content or weak intensity of RGO.[14,24,25] However, the (001) peak is noticed to shift slightly rightward, from 10.5° in pure BiOBr to 10.9° in

https://doi.org/10.1021/acsomega.2c03965
ACS Omega 2022, 7, 35805−35813

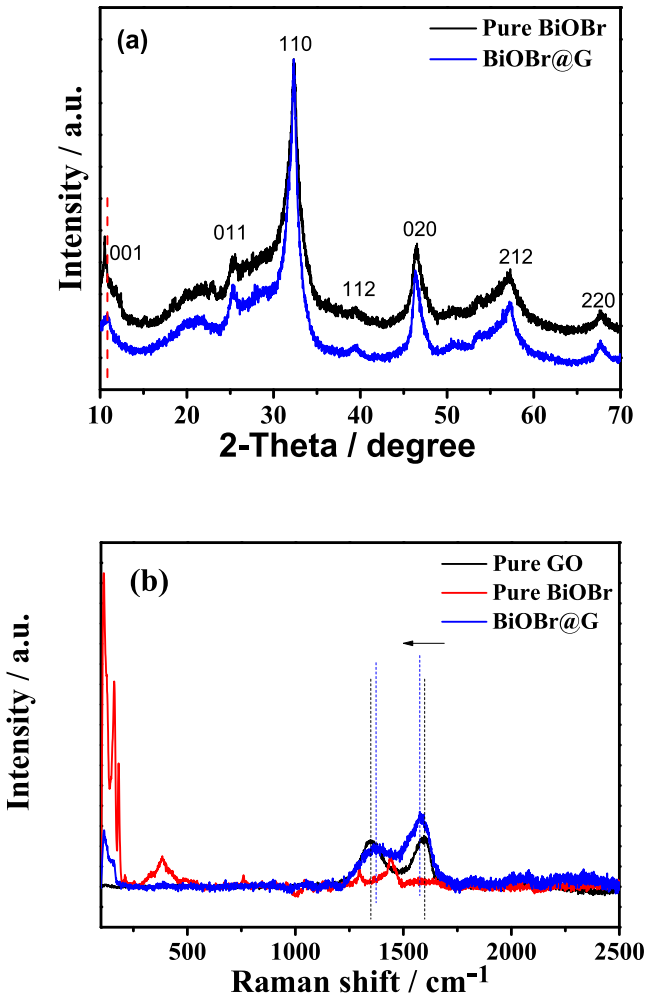

Figure 3. XRD patterns (a) and Raman spectra (b) of a series of samples.

BiOBr@G. In addition, the intensity of the (001) peak is diminished for the BiOBr@G composite in comparison with that of pure BiOBr. Distortion and defects of the BiOBr crystal lattice induced by introduction of the C atom from graphene, suggesting the creation of a coordinated interaction between graphene and the (001) facets of BiOBr subunits, might have been evidenced by the slight shift in the low-intensity (001) diffraction peak.[24] Subsequent characterization of BiOBr@G also supports the presence of graphene.

The formation of the BiOBr@G composite is further confirmed through Raman spectroscopy, and the resulting Raman spectrum is shown in Figure 3b. The A_{1g} internal stretching mode of Bi-Br in BiOBr corresponds to the strong Raman band appearing at 112.2 cm^{-1}.[26,27] Additionally, no obvious Raman signals are observed around 1346 or 1595 cm^{-1} for pure BiOBr. A characteristic peak of BiOBr is also observed at 114.5 cm^{-1} for the BiOBr@G composite. Successful generation of the BiOBr@G composite is further confirmed by two new characteristic peaks appearing at 1367.3 and 1575.9 cm^{-1}, corresponding to the G band (~1575.9 cm^{-1}, E_{2g} phonon of sp^2 carbon atom) and D bands (~1367.3 cm^{-1}, *k*-point phonon of A_{1g} symmetry), respectively.[20]

In contrast to the G band line of 1595.5 cm^{-1} in pure graphene oxide (GO), it is found that the G band line of the BiOBr@G composite shifts toward a lower frequency. This Raman band shift of a specific wavenumber is observed for the BiOBr@G composite while judged against the GO Raman spectra, indicating strong interactions between BiOBr and graphene oxide.[28,29] In addition, while comparing the I_D/I_G value of GO, the D/G intensity ratio of BiOBr@G is found to be obviously decreased from 0.84 for GO to 0.52 for BiOBr@G, indicating the larger size of graphite-like crystalline sp^2 domains. This may be allowed and attributed to less defects and disorders or more sp^2 domains in the graphitized structure and formation of numerous large-sized freshly created in-plane graphite-like crystalline sp^2 domains induced by solvothermal treatment.[20] The above-mentioned characterizations affirm that the reduction of GO and development of the composite of BiOBr/RGO are concurrently accomplished by this synthesis method.

Furthermore, XPS spectra are used to confirm the chemical composition and surface valence states of pure BiOBr and the BiOBr@G composite. We have confirmed the existence of Bi, Br, O, and C elements by surveying the BiOBr@G composite, as shown in Figure 4a.[25] Figure 4b shows two peaks with an interval of 5.3 eV, which are assigned to Bi $4f_{7/2}$ and Bi $4f_{5/2}$ spin−orbital splitting photoelectrons in the Bi^{3+} state,[25] exhibiting Bi 4f core-level spectra of BiOBr (Figure 4b) and BiOBr@G (Figure 4c). The two peaks in the Bi 4f spectrum of pure BiOBr are centered at 160.3 and 165.6 eV, and those for the BiOBr@G composite are found to be centered at 159.9 and 165.2 eV. Hence, the shift in the Bi^{3+} XPS peak position is evident and indicates the probable existence of chemical bonding between BiOBr and graphene oxide. Two additional fitting peaks appearing around 157.6 and 163.3 eV related to Bi $4f_{5/2}$ and Bi $4f_{7/2}$ are further observed (Figure 4c), respectively. These peaks are much smaller than the binding energies of Bi−O and Bi−Br bonds, which further indicates the Bi−C bond formed in the BiOBr@G composite, suggesting a covalent linking between BiOBr and graphene components, and similar findings have also been reported in other previous reports.[11,17]

UV−vis diffuse reflectance spectra (DRS) are used to measure the optical properties of pure BiOBr and the BiOBr@G composite. As shown in Figure 5a, both the pristine BiOBr and BiOBr@G composite show analogous absorption edges at about 435 nm wavelength, indicating the probability of visible light-driven photocatalytic activity. The successful modification of graphene with BiOBr nanoflakes can be reconfirmed by the slightly different absorption edges and comparatively stronger absorption of the BiOBr@G composite than that of pure BiOBr in the visible region due to the increased background absorption by the darker colors of the material.[24] The band gap energy can be additionally calculated by the expression $\alpha(h\upsilon) = A(h\upsilon - E_g)^{n/2}$, where α, h, υ, A, and E_g are the absorption coefficient, Planck's constant, photon frequency, a constant, and energy of the band gap, respectively, and the value of n is 4 for the indirect transition in the case of BiOBr.[9,31] The best-fit curve following the above-mentioned equation to the experimental data (Figure 5b) estimates that the band gaps (E_g) of pure BiOBr and BiOBr@G are almost 2.82 and 2.80 eV, respectively. The absorption edge of the BiOBr@G composite found to remain slightly modified in comparison with that of BiOBr can be attributed to the free distribution of graphene together with the incorporation of carbon atoms in the BiOBr@G composite.[24,25] We have investigated the top valence band (VB) using XPS valence band spectra (Figure 5c). Maximum energies of the valence band (VB) of pure BiOBr and BiOBr@G are 2.48 and 2.23 eV, respectively.

https://doi.org/10.1021/acsomega.2c03965
ACS Omega 2022, 7, 35805−35813

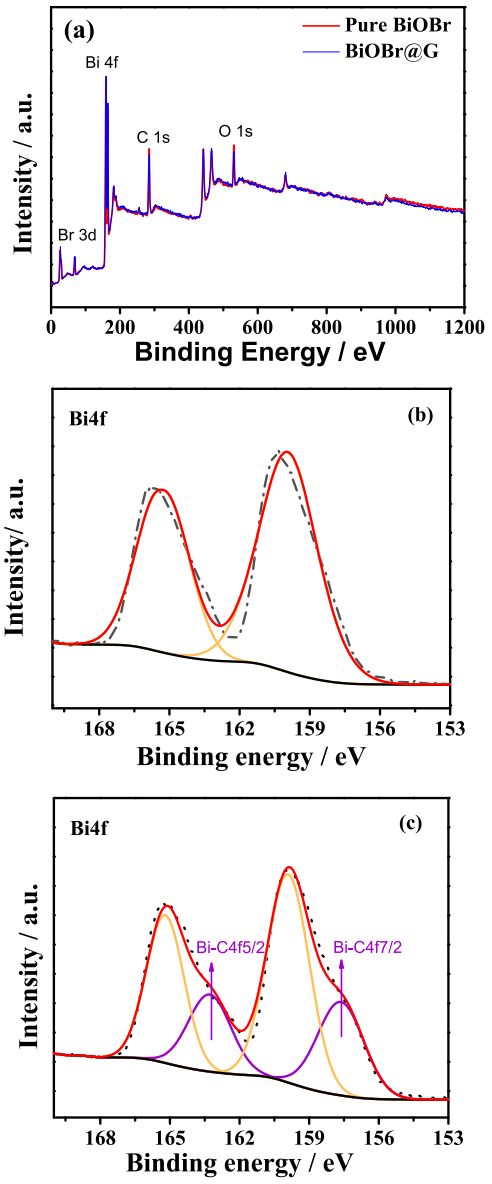

Figure 4. XPS survey spectra for BiOBr and BiOBr@G (a) and Bi 4f core level for BiOBr (b) and BiOBr@G (c).

Correspondingly, the minimum energies of their conduction band (CB) occur at −0.34 and −0.57 eV. Thus, it is noticeable that the CB minimum of BiOBr@G is 0.23 eV more negative than that of pristine BiOBr. The literature reports that the upshifting of the CB facilitates active superoxide species generation by photogenerated electrons and also endorses the transfer of photoexcited electrons to reactants. The process helps prevent electron−hole recombination.[30] Therefore, the composite structural assembly of BiOBr nanoflakes hybridized with freely distributed RGO sheets can effectively enhance light absorption and elevate the CB minimum, which can promote the enhancement of photocatalytic activity.

To assess the visible light-induced charge separation efficiency of the pristine BiOBr and BiOBr@G composite, photocurrents are measured at a light intensity of 100 mw/cm^{-1} for numerous ON/OFF cycles, and the results are depicted in Figure 6a. Figure 6a shows a sharp increase in photocurrent density for both samples under light irradiation, indicating an appreciable photoresponse. Upon comparison of

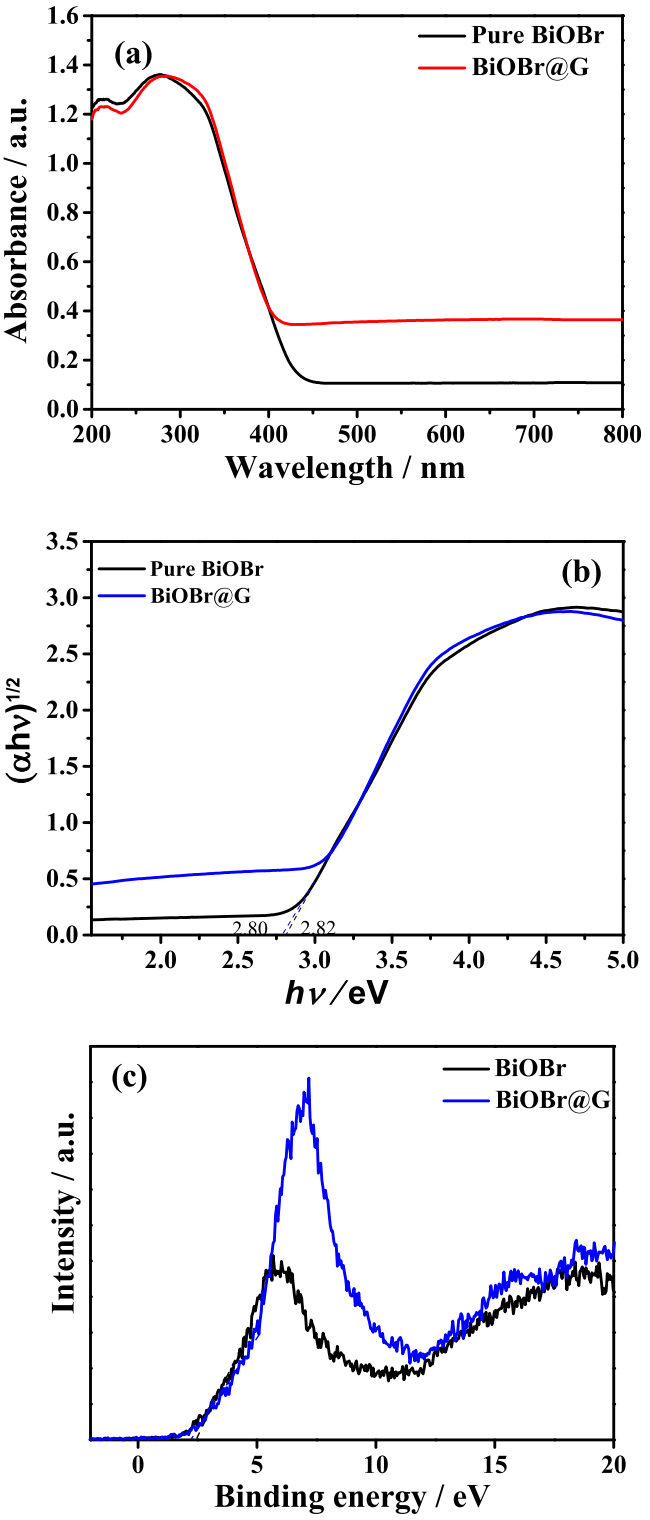

Figure 5. Diffuse reflectance absorption spectra (a) and Tauc plots showing the band gap (b) and XPS valence band spectra (c) of BiOBr and the BiOBr@G composite.

the photocurrent responses, it is obvious that the BiOBr@G composite demonstrates a photocurrent density four times higher than that produced by pure BiOBr flakes, indicating more efficient separation and quicker transfer of photoinduced electrons in the BiOBr@G composite. This result is in agreement with additional PL measurements and strongly supports subsequent results regarding the photodegradation of

https://doi.org/10.1021/acsomega.2c03965
ACS Omega 2022, 7, 35805−35813

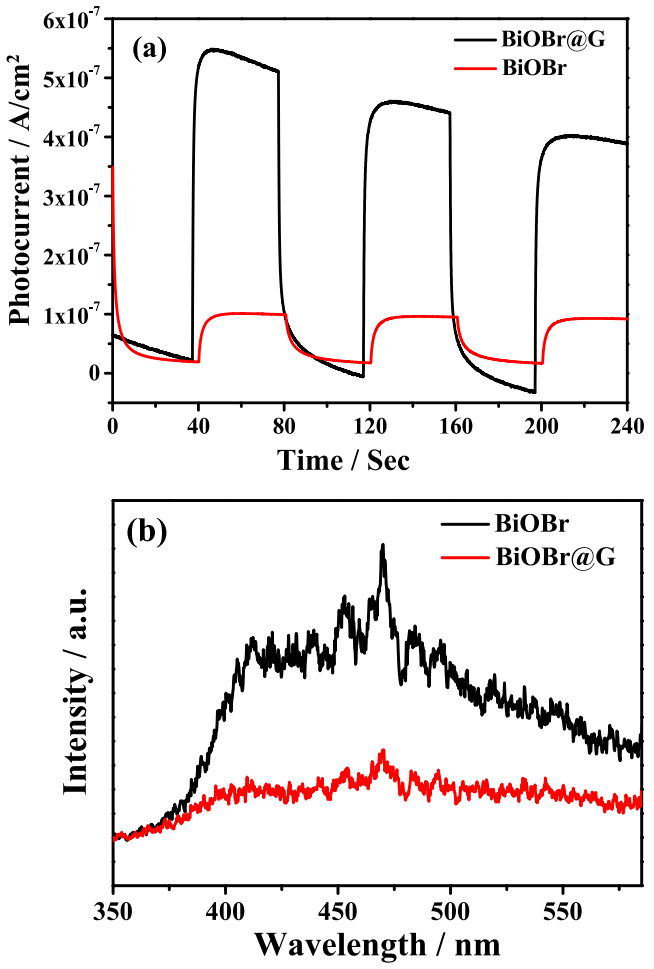

Figure 6. Transient photocurrent response (a) and PL spectra (b) of pure BiOBr and the BiOBr@G composite.

RhB molecules. The recombination efficiency of photogenerated e^- and h^+ for a given photocatalyst can be efficiently analyzed using photoluminescence (PL) emission spectra.[13,31] The results obtained for both the samples at an excitation wavelength of 320 nm are depicted in Figure 6b. Both samples have nearly matching PL emission peaks positioned between 375 and 500 nm. The BiOBr@G composite displays considerable emission quenching compared to that of pure BiOBr, indicating a less efficiency for e^- and h^+ recombination. This phenomenon can be ascribed to their fast transfer ability of electrons from BiOBr to graphene through their close interaction interface, in accordance with the photocurrent results. Thus, sufficient interface connection between graphene and BiOBr flakes plays a vital role in the BiOBr@G composite, where graphene serves as an efficient electron acceptor and transporter due to its two-dimensional conjugation structure and excellent conductivity confirmed indirectly. Therefore, rapid charge transport can be achieved, and an effective charge carrier separation can also be subsequently accomplished. Hence, the lifetime of the charge carriers is extended, resulting in an enhancement in the photocatalyst activity. Based on these experimental results, we conclude that the unique morphology and microstructure of the BiOBr@G composite endorse the creation, splitting, and transportation of electron−hole pairs, underlining its improved photocatalytic performance. The obtainability of electrons in said samples is confirmed by the photocurrent measurements. Electron and hole scavenging experiments are performed to verify their presence for degradation, which is discussed below.

The photocatalytic performance of pure BiOBr and BiOBr@G composites has been evaluated by the photodegradation of the RhB contaminant under visible light (≥420 nm), Figure 7.

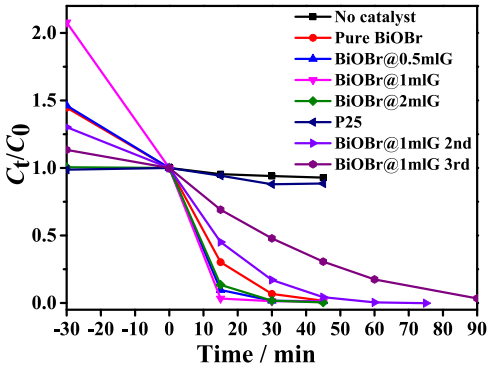

Figure 7. Photodegradation of RhB under visible light ($\lambda \geq 420$ nm) for a series of samples and stability performance of the BiOBr@G-1mL composite.

We have monitored the concentration changes (C_t/C_0) of the RhB dye (553 nm) in aqueous solution through the variation of absorbance (A_t/A_0) over different time intervals.[17] Here, C_0 and A_0 indicate the concentration and absorbance of the RhB dye before irradiation in the presence of the photocatalyst after adsorption equilibrium, respectively, and C_t and A_t mean the concentration and absorbance of the aqueous solution of the RhB dye after different irradiation times, respectively. The blank sample clearly demonstrates that direct photolysis of RhB molecules is negligible without photocatalysts. After 15 min of visible light irradiation, the BiOBr@G-1mL composite photodegrades almost 97% of RhB molecules, compared to only 70% for pure BiOBr, to the best of our knowledge, which is quite superior to that of previous studies.[7,9,12,32] In comparison, the BiOBr@G-1mL composite with an optimal combination of GO mass displays the highest photocatalytic activity among a series of BiOBr@G composites with different graphene oxide contents, which are ordered as BiOBr@G-1mL > BiOBr@G-0.5mL (BiOBr@G-2mL) > pure BiOBr > P25. Therefore, it is easy to conclude that the degradation efficiency of RhB molecules can be improved compared to that of pure BiOBr after graphene modification on BiOBr flake systems. The above-mentioned results demonstrate satisfactorily that the BiOBr@G composite in its present structure may induce a synergistic effect, producing efficient light absorption for more photogenerated carriers and extra-strong interactions due to covalent bonding of Bi−C between BiOBr and graphene for faster charge separation and transfer efficiency, which are responsible for the enhancement of the photodegradation process of the RhB dye. Reliable reusability in performance is critically important for real-life applications of photocatalysts. The photocatalytic stability of the BiOBr@G-1mL composite is evaluated by recycle experiments named as BiOBr@G-1mL 2nd and BiOBr@G-1mL 3rd. As shown in Figure 7, although the degradation time of BiOBr@G-1mL of RhB increases to 60min for the 2nd recycle run and 90 min for the 3rd recycle run, almost complete degradation can still be attained with a very low input of the BiOBr@G-1mL photocatalyst in comparison with the first run after recycling runs. More

https://doi.org/10.1021/acsomega.2c03965
ACS Omega 2022, 7, 35805−35813

importantly, the photodegradation efficiency of BiOBr@G-1mL has not been changed with increasing duration of exposure. This may be mainly related to the low amount of the sample together with mass loss in recycling.

To explore the photodegradation mechanism of the BiOBr@G photocatalyst for the RhB dye, a series of photodegradation experiments adding different scavengers are performed using a technique similar to that narrated in the above-mentioned photodegradation experiment with RhB dye pollutants, as depicted in Figure 8a. We have also witnessed that when 0.2 mM silver nitrate (e^- scavenger) is added, the photocatalytic efficiency is considerably diminished to 52%, suggesting that e^- is the major source of ROS in the photocatalysis method.[25,33] Similarly, in the presence of a superoxide radical ($\bullet O_2$) scavenger (benzoquinone), a hole (h^+) scavenger (methanol), and a hydroxyl radical ($\bullet$OH) scavenger (t-butanol), RhB photodegradation rates are suppressed to 67, 86, and 92%, respectively, indicating that h^+ and $\bullet O_2-$ radicals contribute largely to the high photocatalytic ability, while $\bullet$OH radicals do so only minimally.[20,25] In addition, to confirm the radicals generated by the photodegradation process, the ESR spectra of the pure BiOBr and BiOBr@G catalyst have also been detected, as shown in Figure 8b. Compared to the signals identified from the samples in the dark, ESR signals of DMPO-$O_2\bullet-$ could be clearly detected when the pure BiOBr and BiOBr@G suspensions are exposed to visible light; however, a relatively stronger ESR signal in the BiOBr@G suspension is found compared to that of the pure BiOBr suspension, which specifies that the BiOBr@G catalyst can be efficiently agitated by visible light to generate more photoinduced electrons and holes, furthermore reacting with adsorbed oxygen/H_2O to generate $\bullet O_2-$ on the photocatalyst surface.

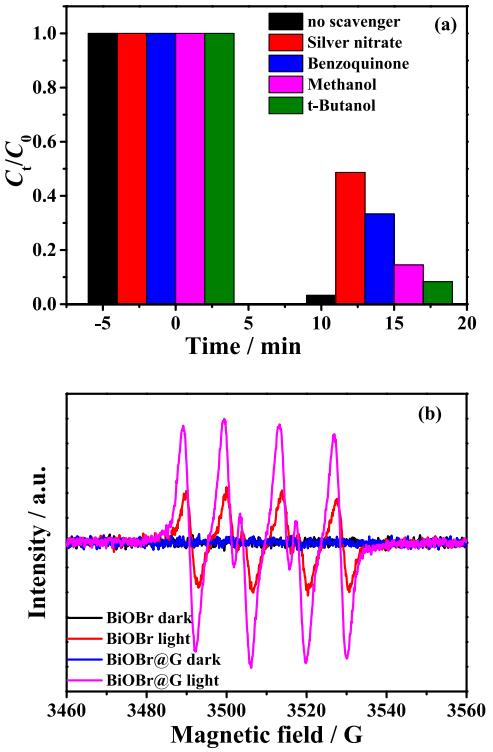

Figure 8. Photodegradation dynamics of RhB in the presence of BiOBr@G with and without the addition of a series of scavengers (a) and ESR spectra (b: superoxide radical) of pure BiOBr and the BiOBr@G composite.

According to the literature, the work function of the VB and CB of BiOBr is usually less than the ground (−5.45 eV) and excited potential (−3.08 eV) of the RhB dye, and the potential of graphene lies around −4.42 eV; thus, direct electron transfer from RhB* to graphene appears favorable from the viewpoint of thermodynamics and feasible than that of BiOBr in BiOBr@G.[25,34] In accordance with the literature reports and above-mentioned discussion, a reasonable mechanism to interpret the exceptional catalytic properties of the BiOBr@G catalyst is proposed as follows. Under visible light irradiation, RhB dye molecules are excited to RhB* and more easily transport electrons into the CB of BiOBr@G due to the elevation of the CB minimum via RGO graphene; also, BiOBr flakes can also be excited to produce photoinduced electrons and holes.[23,25] Then, photogenerated electrons (e^-) on the conduction band (CB) of BiOBr, which is also upshifted by the insertion of RGO sheets, thus efficiently transfer and diminish electron−hole recombination on the surface of BiOBr and quickens the photocatalytic reaction. At the same time, these well-separated electrons are able to reduce O_2 molecules adsorbed on the catalyst surface to $\bullet O_2-$ and decompose RhB molecules into harmless products such as small molecules and others. On the other hand, photogenerated holes (h^+) left in the valence band (VB) of BiOBr can also directly oxidize RhB to produce harmless substances. Overall, the introduction of RGO plays an important role in the enhanced photoactivity of the BiOBr semiconductor photocatalyst for several causes. First, superior properties of BiOBr itself and the introduction of conductive RGO sheets lead to the pronounced visible light harvesting capability of the BiOBr@G composite, causing the creation of greater photoexcited electrons and holes. Second, assembly of graphene and BiOBr with a precise structure and morphology and the interplay between BiOBr flakes and freely assembled RGO sheets make conductive RGO sheets a more efficient acceptor for electron transfer, easing charge transportation, and hindering electron−hole recombination in the BiOBr@G composite. Both synergistic effects act to the increase the photocatalytic performance.

4. CONCLUSIONS

In summary, to improve the photocatalytic performance, we have described a novel 2D/2D self-assembled BiOBr@G photocatalyst via a facile hydrothermal process, in which novel BiOBr flakes are first produced in an immiscible solvent system at room temperature without the use of corrosive acids or other expensive chemicals. The structural and morphological characteristics confirmed that BiOBr flakes with a definite structure and morphology can be well modified using self-assembled reduced graphene oxide sheets via covalent interplays of the Bi−C bond and adequate contact of the BiOBr (112) plane and graphene (002) plane, which freely ornament the surface of BiOBr flakes or are noticed in them. This microstructure and micromorphology of the BiOBr@G composite result in pronounced visible light absorption and further efficient partition and transportation of photogenerated electrons and holes, providing only a small amount of the obtained BiOBr@G composite (5 mg) with enhanced visible degradation efficiency for the RhB dye with a greater concentration of 20 mg/mL compared to that of pure BiOBr. Trapping experiments with the active species confirm that electrons are the main source of ROS in the photocatalysis

https://doi.org/10.1021/acsomega.2c03965
ACS Omega 2022, 7, 35805−35813

system, and subsequent generation of $\bullet O^2$ radicals and h^+ contributes to the oxidation of RhB molecules. This investigation reports a new facile scheme to enhance the photocatalytic activity of conventional inorganic photocatalysts by alteration with graphene materials to remove pollution in the living environment.

AUTHOR INFORMATION

Corresponding Authors

Weiwei He − *Key Laboratory of Micro-Nano Materials for Energy Storage and Conversion of Henan Province, Institute of Surface Micro and Nano Materials, Xuchang University, Henan 461000, P. R. China;* orcid.org/0000-0002-3495-9514; Email: heweiweixcu@gmail.com

Seung Hee Lee − *Department of Nano Convergence Engineering and Department of Polymer Nano Science and Technology, Jeonbuk National University, Jeonju, Jeonbuk 54896, Korea;* orcid.org/0000-0001-5943-9788; Email: lsh1@jbnu.ac.kr

Authors

Weiwei Tie − *Key Laboratory of Micro-Nano Materials for Energy Storage and Conversion of Henan Province, Institute of Surface Micro and Nano Materials, Xuchang University, Henan 461000, P. R. China*

Surjya Sarathi Bhattacharyya − *Asutosh College, Kolkata 700 026 West Bengal, India*

Cancan Han − *Key Laboratory of Micro-Nano Materials for Energy Storage and Conversion of Henan Province, Institute of Surface Micro and Nano Materials, Xuchang University, Henan 461000, P. R. China*

Shuaibiao Qiu − *Key Laboratory of Micro-Nano Materials for Energy Storage and Conversion of Henan Province, Institute of Surface Micro and Nano Materials, Xuchang University, Henan 461000, P. R. China*

Complete contact information is available at: https://pubs.acs.org/10.1021/acsomega.2c03965

Notes

The authors declare no competing financial interest.

ACKNOWLEDGMENTS

This research was supported by the Youth Backbone Teacher Funding Project in Universities of Henan Province (2021GGJS145), China; the Key Scientific Research Project Plan in Universities of Henan Province (22A430036), China; the Outstanding Young Backbone Talents Training Program of Xuchang University, China; and the Zhongyuan Thousand Talents Project of Henan Province (204200510016), China. SH Lee would like to thank the support of the National Research Foundation of Korea (NRF) grant funded the Korean government (MSIT) (No. 2019R1A5A8080326).

REFERENCES

(1) Lin, J. Y.; Ye, W. Y.; Huang, J.; Ricard, B.; Baltaru, M. C.; Greydanus, B.; Balta, S.; Shen, J. N.; Vlad, M.; Sotto, A.; et al. Toward resource recovery from textile wastewater: dye extraction, water and base/acid regeneration using a hybrid NF-BMED process. *ACS Sustainable Chem. Eng.* **2015**, *3*, 1993−2001.

(2) Liu, L. Y.; Yang, C.; Tan, W.; Wang, Y. Degradation of acid red 73 by activated persulfate in a heat/Fe_3O_4@AC system with ultrasound intensification. *ACS Omega* **2020**, *5*, 13739−13750.

(3) Chen, X.; Zhang, X.; Li, Y. H.; Qi, M. Y.; Li, J. Y.; Tang, Z. R.; Zhou, Z.; Xu, Y. J. Transition metal doping BiOBr nanosheets with oxygen vacancy and exposed {102} facets for visible light nitrogen fixation. *Appl. Catal. B* **2021**, *281*, No. 119516.

(4) Zhao, J. L.; Miao, Z. R.; Zhang, Y. F.; Wen, G. Y.; Liu, L. H.; Wang, X. X.; Cao, X. Z.; Wang, B. Y. Oxygen vacancy-rich hierarchical BiOBr hollow microspheres with dramatic CO_2 photoreduction activity. *J. Colloid Interface Sci.* **2021**, *593*, 231−243.

(5) Patra, A. K.; Kundu, S. K.; Bhaumik, A.; Kim, D. Morphology evolution of single-crystalline hematite nanocrystals: magnetically recoverable nanocatalysts for enhanced facet-driven photoredox activity. *Nanoscale* **2016**, *8*, 365−377.

(6) Tripathy, S. P.; Subudhi, S.; Ray, A.; Behera, P.; Bhaumik, A.; Parida, K. Mixed-valence bimetallic Ce/Zr MOF-based nano-architecture: A visible-light-active photocatalyst for ciprofloxacin degradation and hydrogen evolution. *Langmuir* **2022**, *38*, 1766−1780.

(7) Hussain, A.; Hou, J. H.; Tahir, M.; Wang, X. Z.; Qadri, M. U.; Jiang, T.; Tu, X. Y.; Zhang, T. T.; Dou, Q.; Zou, J. J. Fine-tuning internal electric field of BiOBr for suppressed charge recombination. *J. Environ. Chem. Eng.* **2021**, *9*, No. 104766.

(8) Zhao, G. Q.; Hu, J.; Zou, J.; Long, X.; Jiao, F. P. Modulation of BiOBr-based photocatalysts for energy and environmental application: A critical review. *J. Environ. Chem. Eng.* **2022**, *10*, No. 107226.

(9) Cao, G.; Liu, Z. S.; Feng, P. Z.; Zhao, Y. L.; Niu, J. N. Concave ultrathin BiOBr nanosheets with the exposed {001} facets: room temperature synthesis and the photocatalytic activity. *Mater. Chem. Phys.* **2017**, *199*, 131−137.

(10) Zhu, S. R.; Qi, Q.; Fang, Y.; Zhao, W. N.; Wu, M. K.; Han, L. Covalent triazine framework modified BiOBr nanoflake with enhanced photocatalytic activity for antibiotic removal. *Cryst. Growth Des.* **2018**, *18*, 883−891.

(11) Gao, F. D.; Zeng, D. W.; Huang, Q. W.; Tian, S. Q.; Xie, C. S. Chemically bonded graphene/BiOCl nanocomposites as high-performance photocatalysts. *Phys. Chem. Chem. Phys.* **2012**, *14*, 10572−10578.

(12) Xu, H. F.; Xu, Z. C.; Zhou, J.; Yan, G.; Li, X. W.; Zhou, S. P. Hydrothermal fabrication of BiOBr/magnetic reduced graphene oxide composites with efficient visible light photocatalytic activity. *Ceram. Int.* **2019**, *45*, 15458−15465.

(13) Yao, Y.; Liang, J. X.; Wei, Y.; Zheng, X. K.; Xu, X. Y.; He, G. Y.; Chen, H. Q. One-pot synthesis of visible-light-driven photocatalyst for degradation of rhodamine B: graphene based bismuth/bismuth(III) oxybromide. *Mater. Lett.* **2019**, *240*, 246−249.

(14) Liu, X. Q.; Cai, L. A novel double Z-scheme BiOBr-GO-polyaniline photocatalyst: Study on the excellent photocatalytic performance and photocatalytic mechanism. *Appl. Surf. Sci.* **2019**, *483*, 875−887.

(15) Tie, W. W.; Du, Z. Y.; Yue, H. W.; Bhattacharyya, S. S.; Zheng, Z.; He, W. W.; Lee, S. H. Self-assembly of carbon nanotube/graphitic-like flake/BiOBr nanocomposite with 1D/2D/3D heterojunctions for enhanced photocatalytic activity. *J. Colloid Interface Sci.* **2020**, *579*, 862−871.

(16) Li, X.; Yu, J. G.; Wageh, S.; Al-Ghamdi, A. A.; Xie, J. Graphene in photocatalysis: a review. *Small* **2016**, *12*, 6640−6696.

(17) Tu, X. M.; Luo, S. L.; Chen, G. X.; Li, J. H. One-pot synthesis, characterization, and enhanced photocatalytic activity of a BiOBr-graphene composite. *Chem. − Eur. J.* **2012**, *18*, 14359−14366.

(18) Zhang, H.; Lv, X. J.; Li, Y. M.; Wang, Y.; Li, J. H. P25-graphene composite as a high performance photocatalyst. *ACS Nano* **2010**, *4*, 380−386.

(19) Li, Q.; Guo, B. D.; Yu, J. G.; Ran, J. R.; Zhang, B. H.; Yan, H. J.; Gong, J. R. Highly efficient visible-light-driven photocatalytic hydrogen production of CdS-cluster-decorated graphene nanosheets. *J. Am. Chem. Soc.* **2011**, *133*, 10878−10884.

(20) Chen, Y.; Sun, F. Q.; Huang, Z. J.; Chen, H.; Zhuang, Z. Z.; Pan, Z.; Long, J. F.; Long, J.; Gu, F. L. Photochemical fabrication of SnO_2 dense layers on reduced graphene oxide sheets for application in photocatalytic degradation of p-Nitrophenol. *Appl. Catal., B* **2017**, *215*, 8−17.

(21) Yu, X.; Shi, J. J.; Feng, L. J.; Li, C. H.; Wang, L. A three-dimensional BiOBr/RGO heterostructural aerogel with enhanced and selective photocatalytic properties under visible light. *Appl. Surf. Sci.* **2017**, *396*, 1775−1782.
(22) Zhang, X. Q.; Feng, Y. Y.; Tang, S. D.; Feng, W. Preparation of a graphene oxide-phthalocyanine hybrid through strong π-π interactions. *Carbon* **2010**, *48*, 211−216.
(23) Allagui, L.; Chouchene, B.; Gries, T.; Medjahdi, G.; Girot, E.; Framboisier, X.; Amara, A. B. H.; Balan, L.; Schneider, R. Core/shell rGO/BiOBr particles with visible photocatalytic activity towards water pollutants. *Appl. Surf. Sci.* **2019**, *490*, 580−591.
(24) Wei, X. X.; Chen, C. M.; Guo, S. Q.; Guo, F.; Li, X. M.; Wang, X. X.; Cui, H. T.; Zhao, L. F.; Li, W. Advanced visible-light-driven photocatalyst BiOBr-TiO_2-graphene composite with graphene as a nano-filler. *J. Mater. Chem. A* **2014**, *2*, 4667−4675.
(25) Liu, C.; Dong, X. L.; Hao, Y. C.; Wang, X. Y.; Ma, H. C.; Zhang, X. F. Efficient photocatalytic dye degradation over Er-doped BiOBr hollow microspheres wrapped with graphene nanosheets: enhanced solar energy harvesting and charge separation. *RSC Adv.* **2017**, *7*, 22415−22423.
(26) Li, Y. H.; Lai, Z.; Huang, Z. J.; Wang, H. Y.; Zhao, C. X.; Ruan, G. H.; Du, F. Y. Fabrication of BiOBr/MoS_2/graphene oxide composites for efficient adsorption and photocatalytic removal of tetracycline antibiotics. *Appl. Surf. Sci.* **2021**, *550*, No. 149342.
(27) Ghorai, K.; Bhattacharjee, M.; Mandal, D.; Hossain, A.; Bhunia, T.; Das, M.; Ray, P. P.; Show, B.; Bera, P.; Mandal, T. K.; et al. Facile synthesis of $CuCr_2O_4$/BiOBr composite and its photocatalytic activity towards RhB and tetracycline hydrochloride degradation under household visible LED light irradiation. *J. Alloys Compd.* **2021**, *867*, No. 157947.
(28) Hossain, M. M.; Ku, B. C.; Hahn, J. R. Synthesis of an efficient white-light photocatalyst composite of graphene and ZnO nano-particles: Application to methylene blue dyedecomposition. *Appl. Surf. Sci.* **2015**, *354*, 55−65.
(29) Chen, F. J.; Cao, Y. L.; Jia, D. Z.; Liu, A. J. Solid-state synthesis of ZnS/graphene nanocomposites with enhanced photocatalytic activity. *Dyes Pigm.* **2015**, *120*, 8−14.
(30) Chen, J.; Guan, M. L.; Cai, W. Z.; Guo, J. J.; Xiao, C.; Zhang, G. K. The dominant {001} facet-dependent enhanced visible-light photoactivity of ultrathin BiOBr nanosheets. *Phys. Chem. Chem. Phys.* **2014**, *16*, 20909.
(31) Zhao, C. H.; Li, W.; Liang, Y.; Tian, Y.; Zhang, Q. Y. Synthesis of BiOBr/carbon quantum dots microspheres with enhanced photoactivity and photostability under visible light irradiation. *Appl. Catal., A* **2016**, *527*, 127−136.
(32) Yue, J.; Wen, G. C.; Ren, G. N.; Tang, S. W.; Ge, B.; Zhao, L. M.; Shao, X. Superhydrophobic self-supporting BiOBr aerogel for wastewater purification. *Langmuir* **2021**, *37*, 406−416.
(33) Ghosh, S.; Rashmi, D.; Bera, S.; Basu, R. N. Functionalized conjugated polymer with plasmonic Au nanoalloy for photocatalytic hydrogen generation under visible-NIR. *Int. J. Hydrogen Energy* **2019**, *44*, 13262−13272.
(34) Li, B.; Cao, H. Q. ZnO@graphene composite with enhanced performance for the removal of dye from water. *J. Mater. Chem. A* **2011**, *21*, 3346−3349.

https://doi.org/10.1021/acsomega.2c03965
ACS Omega 2022, 7, 35805−35813